Evidence for multifilamentary valence changes in resistive switching SrTiO3 devices detected by transmission X-ray microscopy

A. Koehl, H. Wasmund, A. Herpers, P. Guttmann, S. Werner, K. Henzler, H. Du, J. Mayer, R. Waser, and R. Dittmann

Citation: APL Materials **1**, 042102 (2013); doi: 10.1063/1.4822438
View online: http://dx.doi.org/10.1063/1.4822438
View Table of Contents: http://scitation.aip.org/content/aip/journal/aplmater/1/4?ver=pdfcov
Published by the AIP Publishing

APL MATERIALS **1**, 042102 (2013)

Evidence for multifilamentary valence changes in resistive switching $SrTiO_3$ devices detected by transmission X-ray microscopy

A. Koehl,[1,a] H. Wasmund,[1] A. Herpers,[1] P. Guttmann,[2] S. Werner,[2] K. Henzler,[2] H. Du,[3] J. Mayer,[3] R. Waser,[1,4] and R. Dittmann[1]
[1]*Peter Grünberg Insitute 7, Research Center Jülich, 52428 Jülich, Germany*
[2]*Helmholtz-Zentrum für Materialien und Energie GmbH, Institute for Soft Matter and Functional Materials, Albert-Einstein-Str. 15, 12489 Berlin, Germany*
[3]*Ernst Ruska-Centre (ER-C) for Microscopy and Spectroscopy with Electrons, Research Center Juelich, 52425 Juelich, Germany*
[4]*IWE 2 & JARA-FIT, RWTH Aachen University, 52056 Aachen, Germany*

(Received 12 July 2013; accepted 23 August 2013; published online 1 October 2013)

Transmission X-ray microscopy is employed to detect nanoscale valence changes in resistive switching $SrTiO_3$ thin film devices. By recording Ti L-edge spectra of samples in different resistive states, we could show that some spots with slightly distorted structure and a small reduction to Ti^{3+} are already present in the virgin films. In the ON-state, these spots are further reduced to Ti^{3+} to different degrees while the remaining film persists in the Ti^{4+} configuration. These observations are consistent with a self-accelerating reduction within pre-reduced extended growth defects. [http://dx.doi.org/10.1063/1.4822438]

In recent years resistive switching in transition metal oxides received a lot of research interest due to the proposed application as resistive random access memory (RRAM).[1–3] In material systems which are classified as valence change materials (VCM) the resistive switching process is usually attributed to the diffusion of oxygen vacancies driven by the applied voltage and an associated valence change of the transition metal cations. While these models can explain the macroscopic resistive switching behavior, microscopic details are still unknown. Spectroscopy can be used to directly monitor the relevant valence change,[4–6] but in order to study the presumably filamentary resistive switching process[7–10] within a complete metal-insulator-metal (MIM) structure a significant information depth as well as a high lateral resolution is required. Therefore, NEXAFS-transmission X-ray microscopy (TXM) is a powerful tool as it probes the whole film volume with a lateral resolution down to 25 nm.[11] For NEXAFS-TXM experiments photon transparent samples with a thickness below 100 nm are irradiated by photons in the soft X-ray regime. Fresnel lenses are used as objectives to obtain a magnified image of the sample. Spectroscopic information can be gained by tuning the incident photon energy. In contrast to almost any other technique it is therefore possible to investigate both interfaces of the MIM structure. On the field of resistive switching up to now X-ray microscopy studies have only been reported for the investigation of polycrystalline devices which have been deposited on thin Si_3N_4 membranes.[5,12]

In this work we will employ bulk-sensitive NEXAFS-TXM to study the valence change in resistive switching devices based on single-crystalline $SrTiO_3$ thin films. Although industrial RRAM focus on amorphous or polycrystalline films grown on CMOS compatible Si, epitaxial films are very useful as a model system due to the absence of grain boundaries and a more defined defect

[a]E-mail: a.koehl@fz-juelich.de

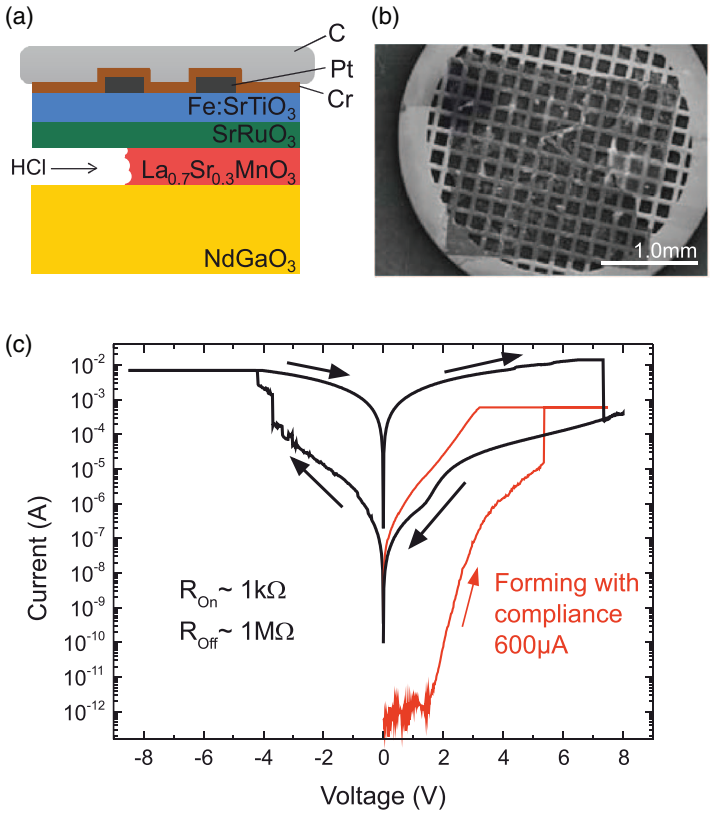

FIG. 1. (a) Multi-layer sample design to detach active device from the substrate for TXM measurements. (b) SEM image of detached carbon support layer with MIM structures on a TEM grid. (c) Bipolar resistive switching with counter-eightwise polarity.

structure.[13, 14] In order to combine the need for a single crystalline growth template with a final sample thickness below 100 nm a new sample preparation is developed.

The preparation of single crystalline films suited for transmission experiments is based on a multi-layer sample design as depicted in Fig. 1(a). The epitaxial films are grown by pulsed laser deposition (see the supplementary material[15] for detailed growth conditions). Starting from a commercially available $NdGaO_3$ (NGO) substrate (CrysTec GmbH, Berlin) we first deposit 100 nm of $La_{0.7}Sr_{0.3}MnO_3$ (LSMO), which will later be used as a sacrificial layer. Subsequently, 15 nm $SrRuO_3$ (SRO) and 20 nm 5%Fe:$SrTiO_3$ (STO) are grown, which will act as bottom electrode and active film, respectively. Due to the small lattice mismatch of these (pseudo)cubic perovskite materials epitaxial growth can be achieved for all three films which has been confirmed by X-ray diffraction. Atomic-force microscopy proves a smooth film surface with a root mean square roughness of 0.4 nm. For the preparation of the top electrodes, 8 nm of Pt is sputter-deposited and lithographically patterned to pads of 10 μm × 10 μm.

For electrical characterization, the SRO layer, which shows metallic conduction, is contacted via wire bonding and the Pt pads are contacted directly with probing needles. The initially large resistance is irreversibly transformed to the MΩ-regime by a forming sweep with 600 μA compliance (see Fig. 1(c)). Afterwards bipolar resistive switching with "counter-eightwise" polarity[10] over roughly three orders of magnitude and with good pad-to-pad reproducibility is observed. By automatic stepping several pads are set into the ON-state.

After preparation and electrical treatment of the switching device, the necessary sample thickness for NEXAFS-TXM below 100 nm is achieved by separating the MIM structure from the substrate by a sample preparation which is inspired by the extraction replica technique.[16] In a first step the switched MIM-structure is covered via sputter deposition with a 5 nm chromium adhesion layer. Afterwards a supporting carbon layer of roughly 40 nm is deposited on top by cathodic arc

evaporation. In order to detach the MIM-structure from the NGO substrate we utilize highly selective chemical etching with hydrochloric acid (HCl). While HCl will dissolve LSMO, the etching rate on STO is expected to be extremely slow.[17] According to literature[18,19] and experimental tests on our samples the etching of SRO is also significantly below the SRO film thickness on the time scales used for etching. Therefore, we maintain both relevant interfaces of the MIM structure.

In order to etch the samples, the whole sample stack is exposed to HCl vapor by mounting it above a beaker of fluid HCl, which is heated to 80 °C (for more details about the etching process see the supplementary material[15]). During etching in HCl vapor no visible changes are observed, but when the sample is transferred into water after 15 min large flat pieces of carbon film with MIM structures are immediately detached from the substrate (probably due to surface tension effects). Figure 1(b) shows a scanning electron microscope (SEM) image of a detached carbon layer which supports the MIM structures on a TEM grid.

The NEXAFS-TXM study was performed at the U41-XM beamline at the BESSY II electron storage ring operated by the Helmholtz-Zentrum Berlin. At this endstation, Ti L-edge spectra can be measured with a spectral resolution of up to $E/\Delta E = 10^4$ and a spatial resolution of 25 nm.[11] In order to record spectra with sufficient signal to noise ratio for each photon energy five separate images are acquired and summed up. Additionally the spectra are normalized by a nearby reference signal without Ti-signature to account for inhomogeneities in the beam intensity.

Figure 2(a) presents a TXM image at the Ti-resonance with a photon energy of $h\nu = 458.0$ eV of a typical virgin sample. Dark contrast is due to the absorption in the STO thin film. Due to adhesion problems (see the supplementary material[15] for details) the pads are usually not completely preserved on the support layer, but typically one can find some homogeneous areas of STO as well as several small "spots" of roughly 80–200 nm which also show strong Ti contrast. These spots are observed on ON as well as Virgin pads and therefore are a result of the thin film preparation. Lenser *et al.*[20] observed extended growth defects of comparable size on $SrTiO_3$ thin films grown by PLD and explained it by a preferred nucleation at the exits of screw dislocations on the substrate. We assume that similar growth defects in our film are the reason for these spotlike structures. The effect might even be enhanced by the subsequent growth of three different perovskite layers as the lattice mismatch might induce additional defect sites. The enhanced contrast (darker color in Fig. 2(a)) of the growth defect compared to the film can be explained by an increased sample thickness as additional material is accumulated at the growth defect.[20] With energy dispersive X-ray spectroscopy we confirmed the presence of Pt and Ru on all regions with Ti contrast, which demonstrates that the complete stack is preserved and contributes to the NEXAFS-TXM signal.

On a virgin pad the Ti L-edge spectra of the homogeneous film as well as the growth defect reveal the typical absorption characteristic of a Ti^{4+} configuration in STO in good agreement with literature[21,22] (see Fig. 2(b)). The Ti L-edge is caused by the excitation of electrons from 2p into 3d level and shows four well separated main lines due to the spin-orbit splitting into L_2 and L_3 lines and the crystal-field splitting into t_{2g} and e_g lines in octahedral symmetry.[23] Direct comparison of the spectra reveals a general increase of the full-width-half-maximum (FWHM) of the e_g lines for the spectra of the growth defects. For the L_3 lines we quantitatively observe a broadening from $FWHM(L_3)_{film} = 0.5$ eV to $FWHM(L_3)_{defect} = 0.7 \ldots 0.9$ eV. In octahedral symmetry the e_g orbitals point to the ligands and are therefore more strongly bound than the t_{2g} orbitals which point in between the ligands.[23] This stronger hybridization of the e_g orbitals can explain why variations of the spectral line shape upon changes of the chemical environment (see Figs. 2 and 3) are mainly concentrated on the e_g lines. The observed broadening of the e_g lines could be a signature of a slightly reduced long range order within the growth defect while the local structure is still dominated by the Ti^{4+} configuration in perovskite lattice geometry.[23,24] Additionally, on some defects a small shift (below 100 meV) of the e_g lines to lower photon energies is detected. The interpretation of this shift will be discussed later in combination with the results on the switched pads.

After characterization of the virgin pads we will now move on to the analysis of the pads which have been set into the ON-state. The homogeneous parts of the film have an identical Ti-signature of a pure Ti^{4+} configuration as observed for the virgin area. However, for the spectra of the extended growth defects clear variations occur. In Fig. 3(a) the spectra of several defects within one pad in the ON-state are presented. Significant variations in the spectral shape are apparent, mainly concentrated

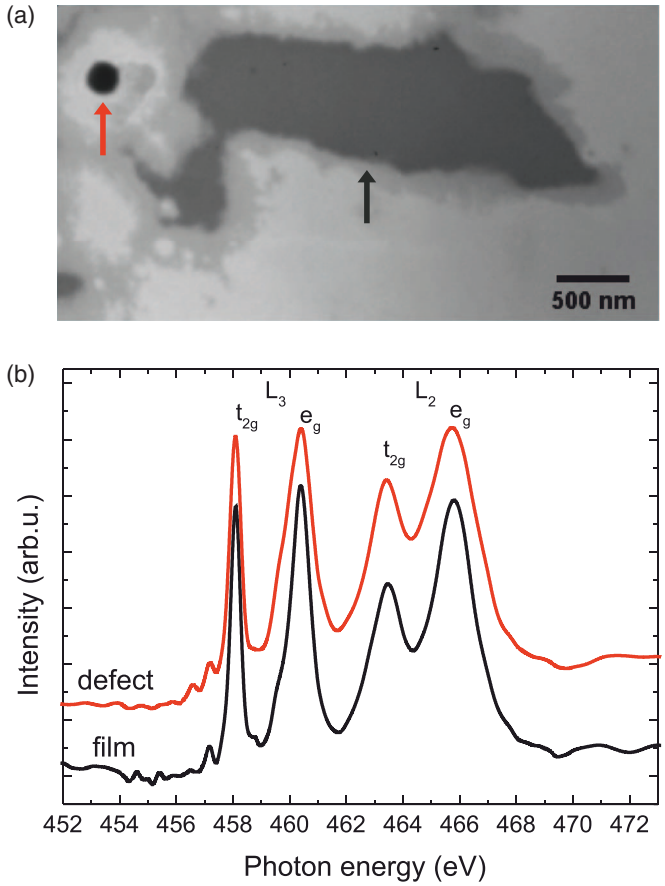

FIG. 2. (a) TXM-image of a virgin pad at hν = 458.0 eV. Dark contrast reveals parts of the STO film, which are attached to the support layer. A homogeneous area of the film (marked by right black arrow) as well as a growth defect (marked by left red arrow) is visible. (b) Comparison of Ti L-edge spectra of the film and the growth defect reveal a broadening of the e_g lines in the defect spectrum.

on the e_g lines. An additional peak arises at the lower photon energy side of the L_3 e_g peak, which is observed as shoulder next to the original peak or a shift of the line. Moreover, the L_2 e_g line is shifted to lower photon energy and the pre-edge features show increased intensity. Generally the observed shifts to lower photon energies indicate a lower valence and therefore the occurrence of Ti^{3+} states.[25–28] The detailed line shape of our results can be compared to literature results of Abbate *et al.*,[22] who presented Ti-XAS spectra for a systematic concentration series $La_{1-x}Sr_xTiO_3$ with x = 0. . . 1. In this system, which we have used as a reference, substituting of Sr^{2+} ions with La^{3+} ions reduces the original Ti^{4+} to a Ti^{3+} configuration, while maintaining the perovskite structure. This reduction of Ti leads precisely to the effect on the Ti-XAS spectra we observed within the growth defects after switching into the ON-state. Therefore, we can assign the variations in spectral shape of the growth defects after switching into the ON-state to a different degree of reduction of Ti^{4+} to Ti^{3+}. Via the redox-reaction $2Ti^{4+} + O \rightarrow 2Ti^{3+} + V_O^{\cdot\cdot} + \frac{1}{2}O_2(g)$ this reduction is directly connected to the creation of oxygen vacancies. In general XAS-spectra reflect also variations in symmetry and strength of the crystal field and indeed modification of the line shape have been reported upon heavy distortion of STO films.[29] Nevertheless, the distortion due to oxygen vacancies in STO is very small[30] and therefore, compared to the valence change, the effect of crystal field has only a minor effect on the line shape.[31,32]

Based on the spectroscopic results we propose the following model (see Fig. 3(b)): The virgin film consists of a perfect STO thin film containing some extended growth defects. Although the film is slightly disturbed within these growth defects the local structure consists of a perovskite

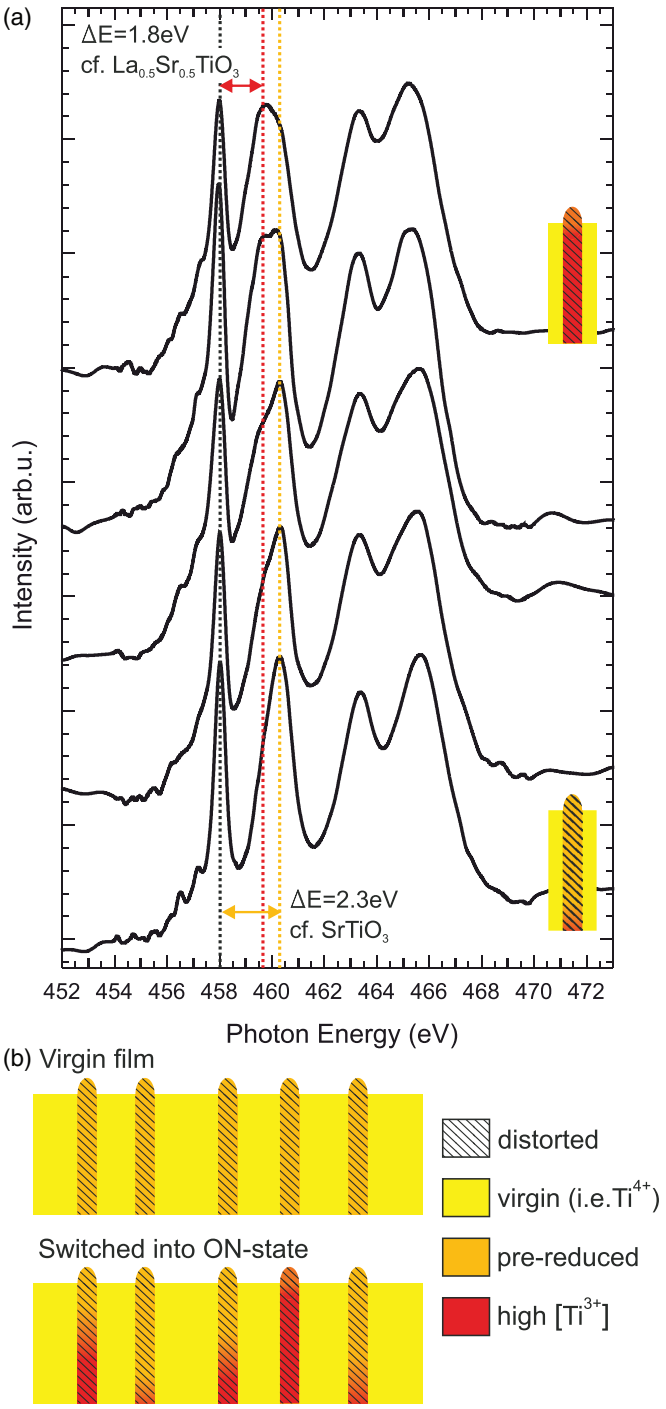

FIG. 3. (a) Ti L-edge spectra of several growth defects located within one pad in the ON-state. Comparison with Ref. 22 reveals reduction to Ti^{3+} to different extent. For the top and bottom spectra the reference material which shows a similar line-shape is indicated. (b) Schematic cross-section model for STO films showing growth defects in the virgin film and reduction to Ti^{3+} after switching into the ON-state.

lattice with Ti^{4+} configuration. As mentioned before, on some of these defects a small shift of the e_g peak position is observed. In line with the results observed at the ON-pad, this could be an indication of a small concentration of Ti^{3+} states within the growth defect. Therefore, we propose that some of the growth defects are pre-reduced already in the virgin state. In accordance to the

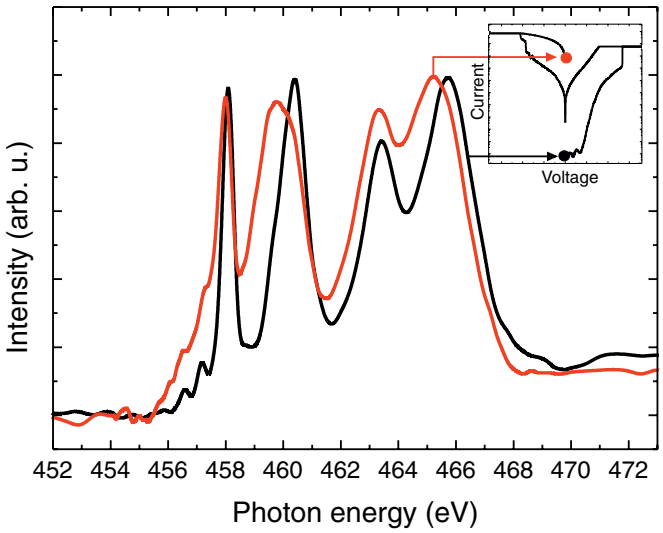

FIG. 4. Ti L-edge spectra of the growth defect with the largest shift of the L_3 e_g peak within a virgin pad (black line) and an ON-pad (red line). For comparison the inset shows the electrical data (for details see Fig. 1(c)). After degradation of the resistance over nine orders of magnitude a clear reduction to Ti^{3+} is visible.

current models for VCM type switching we assume that during forming oxygen is excorporated from the film,[7] which leads to the observed reduction of titanium. Due to the pre-reduction of the film within the growth defects, which goes along with a higher local n-conductivity, the current density inside the defects is increased relative to the film, thus accelerating the oxygen diffusion. Considering the rather high currents in the mA-regime, significant Joule heating in well conducting paths will lead to self-accelerating of the process and therefore small differences of the starting configuration can lead to large variations in the final composition.[33] This can explain that no reduction is obtained in the homogeneous, defect-free film and that different growth defects will show different degrees of reduction.

In terms of the macroscopic electrical behavior, the different filamentary paths within the growth defects constitute a parallel circuit. While at the beginning several growth defects are reduced, due to the self-accelerating process the current will finally concentrate on one single filament. This filament will carry the main current and dominate the overall pad resistance. Therefore, we consider in Fig. 4 the spectrum of the growth defect, which shows the lowest value of the energy position of the L_3 e_g peak of the ON-pad and compare it to the spectrum of a growth defect of the virgin pad. The huge change in resistance over nine orders of magnitude is accompanied by a considerable change in the line shape of the Ti L-edge showing clearly the reduction to Ti^{3+} states. The analysis has been repeated on a second independent pair of virgin and ON-pad and resulted in very similar electrical and spectroscopic results.

The sensitivity of XAS for the crystal field also allows us to study the formation of new phases. For the related system of TiO_2 there is evidence that the resistive switching process is directly connected to the formation of new phases.[34,35] For the STO system, the perovskite lattice can accommodate a Sr deficiency induced by Sr-diffusion to the surface during electrical treatment[9] by the creation of Sr-vacancies. Nevertheless, more severe modifications might lead to a complete phase separation and the formation of TiO_2 or the oxygen deficient Magnéli phases. The observed spectral shape of the growth defects in the virgin film as well as after forming shows good agreement with the $La_{1-x}Sr_xTiO_3$ reference, but cannot be explained by the formation of new phases. In accordance with literature on STO we observe a splitting of the L_3 edge of E_{eg}-$E_{t2g}(L_3) = 2.3$ eV for the virgin film,[21,22] which is reduced during the electrical treatment. In contrast, both TiO_2 phases anatase and rutile show a double peak structure including a significant line with a splitting of more than 2.5 eV.[11,36,37] As no additional intensity is observed at this energy position, we can exclude the formation of TiO_2 phases. The Magnéli phases show very broad spectral features with only two

clearly separated peaks[37] which would be in strong contrast to the observed four-peak structure. Therefore in our system, resistive switching occurs clearly due to a valence change process without any evidence for the formation of new phases.

In conclusion, we have employed NEXAFS transmission X-ray microscopy to investigate the Ti L-edge absorption of resistively switched epitaxial $SrTiO_3$ thin films. Based on wet chemical etching of a sacrificial layer, a new route for sample preparation was developed to allow the combination of a thick single crystalline substrate during thin film growth and a final sample thickness below 100 nm for the transmission experiment. On the virgin film, we observed a spectral shape, which is a signature of perfect Ti^{4+} configuration in perovskite structure. Additionally we find growth defects with a slightly distorted symmetry and very small contributions of Ti^{3+} states. After switching into the ON-state, we observed different degrees of reduction to Ti^{3+} within the growth defects while the film remains in the isolating Ti^{4+} configuration. We propose that these growth defects are significantly reduced to Ti^{3+} during forming. The self-accelerating process will transform one of the growth defects into a completely conductive filament. Comparison with literature data of the Ti L-edge proves the conservation of the perovskite structure during the reduction without any indications for new phase formations. Overall we have been able to trace back the resistance change in a RRAM device to the underlying redox-process and allocate the switching filament to extended growth defects present in the virgin films.

This work has been supported by the Deutsche Forschungsgemeinschaft (DFG) (SFB 917) and COST Action MP0901 "NanoTP." This work was in part funded by the European Union Council under the 7th Framework Program (FP7) Grant No. 246102 IFOX. We thank G. Nitzinger for deposition of the carbon layer and O. Kim for the growth of LSMO layers. We thank HZB for the allocation of synchrotron radiation beamtime and S. Rehbein, HZB, for providing the high-resolution zone plate objectives used for NEXAFS-TXM.

[1] R. Waser, R. Dittmann, G. Staikov, and K. Szot, Adv. Mater. **21**, 2632 (2009).
[2] R. Waser and M. Aono, Nature Mater. **6**, 833 (2007).
[3] D. B. Strukov, G. S. Snider, D. R. Stewart, and R. S. Williams, Nature (London) **453**, 80 (2008).
[4] M. Sowinska, T. Bertaud, D. Walczyk, S. Thiess, M. A. Schubert, M. Lukosius, W. Drube, C. Walczyk, and T. Schroeder, Appl. Phys. Lett. **100**, 233509 (2012).
[5] J. P. Strachan, M. D. Pickett, J. J. Yang, S. Aloni, A. L. David Kilcoyne, G. Medeiros-Ribeiro, and R. Stanley Williams, Adv. Mater. **22**, 3573 (2010).
[6] C. Lenser, A. Kuzmin, J. Purans, A. Kalinko, R. Waser, and R. Dittmann, J. Appl. Phys. **111**, 076101 (2012).
[7] K. Szot, W. Speier, G. Bihlmayer, and R. Waser, Nature Mater. **5**, 312 (2006).
[8] J. P. Strachan, J. J. Yang, R. Münstermann, A. Scholl, G. Medeiros-Ribeiro, D. R. Stewart, and R. S. Williams, Nanotechnology **20**, 485701 (2009).
[9] R. Dittmann, R. Muenstermann, I. Krug, D. Park, T. Menke, J. Mayer, A. Besmehn, F. Kronast, C. M. Schneider, and R. Waser, Proc. IEEE **100**, 1979 (2012).
[10] R. Muenstermann, T. Menke, R. Dittmann, and R. Waser, Adv. Mater. **22**, 4819 (2010).
[11] P. Guttmann, C. Bittencourt, S. Rehbein, P. Umek, X. Ke, G. Van Tendeloo, C. P. Ewels, and G. Schneider, Nat. Photonics **6**, 25 (2012).
[12] J. P. Strachan, G. Medeiros-Ribeiro, J. J. Yang, M.-X. Zhang, F. Miao, I. Goldfarb, M. Holt, V. Rose, and R. S. Williams, Appl. Phys. Lett. **98**, 242114 (2011).
[13] D. J. Keeble, S. Wicklein, L. Jin, C. L. Jia, W. Egger, and R. Dittmann, Phys. Rev. B **87**, 195409 (2013).
[14] D. J. Keeble, S. Wicklein, R. Dittmann, L. Ravelli, R. A. Mackie, and W. Egger, Phys. Rev. Lett. **105**, 226102 (2010).
[15] See supplementary material at http://dx.doi.org/10.1063/1.4822438 for details on PLD growth parameters and sample preparation.
[16] S. Amelinckx, *Handbook of Microscopy: Applications* (VCH, 1997).
[17] L. Pellegrino, M. Biasotti, E. Bellingeri, C. Bernini, A. S. Siri, and D. Marré, Adv. Mater. **21**, 2377 (2009).
[18] D. Weber, R. Vöfély, Y. Chen, Y. Mourzina, and U. Poppe, Thin Solid Films **533**, 43 (2013).
[19] X. D. Wu, S. R. Foltyn, R. C. Dye, Y. Coulter, and R. E. Muenchausen, Appl. Phys. Lett. **62**, 2434 (1993).
[20] C. Lenser, Z. Connell, A. Kovács, R. Dunin-Borkowski, A. Köhl, R. Waser, and R. Dittmann, Appl. Phys. Lett. **102**, 183504 (2013).
[21] A. Koehl, D. Kajewski, J. Kubacki, C. Lenser, R. Dittmann, P. Meuffels, K. Szot, R. Waser, and J. Szade, Phys. Chem. Chem. Phys. **15**, 8311 (2013).
[22] M. Abbate, F. M. F. de Groot, J. C. Fuggle, A. Fujimori, Y. Tokura, Y. Fujishima, O. Strebel, M. Domke, G. Kaindl, J. van Elp, B. T. Thole, G. A. Sawatzky, M. Sacchi, and N. Tsuda, Phys. Rev. B **44**, 5419 (1991).
[23] F. M. F. de Groot, J. C. Fuggle, B. T. Thole, and G. A. Sawatzky, Phys. Rev. B **41**, 928 (1990).
[24] P. Krüger, Phys. Rev. B **81**, 125121 (2010).
[25] F. M. F. de Groot, J. C. Fuggle, B. T. Thole, and G. A. Sawatzky, Phys. Rev. B **42**, 5459 (1990).
[26] A. Ohtomo, D. A. Muller, J. L. Grazul, and H. Y. Hwang, Nature (London) **419**, 378 (2002).

[27] D. A. Muller, N. Nakagawa, A. Ohtomo, J. L. Grazul, and H. Y. Hwang, Nature (London) **430**, 657 (2004).
[28] J.-S. Lee, Y. W. Xie, H. K. Sato, C. Bell, Y. Hikita, H. Y. Hwang, and C.-C. Kao, Nature Mater. **12**, 703 (2013).
[29] E. O. Filatova, A. A. Sokolov, Y. V. Egorova, A. S. Konashuk, O. Y. Vilkov, M. Gorgoi, and A. A. Pavlychev, J. Appl. Phys. **113**, 224301 (2013).
[30] V. E. Alexandrov, E. A. Kotomin, J. Maier, and R. A. Evarestov, Eur. Phys. J. B **72**, 53 (2009).
[31] G. van der Laan and I. W. Kirkman, J. Phys. Condens. Matter **4**, 4189 (1992).
[32] F. M. F. de Groot, M. O. Figueiredo, M. J. Basto, M. Abbate, H. Petersen, and J. C. Fuggle, Phys. Chem. Miner. **19**, 140 (1992).
[33] S. Menzel, B. Klopstra, C. Kügeler, U. Böttger, G. Staikov, and R. Waser, MRS Proceedings **1160**, 1160-H09-03 (2009).
[34] K. Szot, M. Rogala, W. Speier, Z. Klusek, A. Besmehn, and R. Waser, Nanotechnology **22**, 254001 (2011).
[35] D.-H. Kwon, K. M. Kim, J. H. Jang, J. M. Jeon, M. H. Lee, G. H. Kim, X.-S. Li, G.-S. Park, B. Lee, S. Han, M. Kim, and C. S. Hwang, Nat. Nanotechnol. **5**, 148 (2010).
[36] S. O. Kucheyev, T. van Buuren, T. F. Baumann, J. H. Satcher, T. M. Willey, R. W. Meulenberg, T. E. Felter, J. F. Poco, S. A. Gammon, and L. J. Terminello, Phys. Rev. B **69**, 245102 (2004).
[37] E. Stoyanov, F. Langenhorst, and G. Steinle-Neumann, Am. Mineral. **92**, 577 (2007).